VI International Conference on Computational Methods in Marine Engineering
MARINE 2015
F. Salvatore, R. Broglia and R. Muscari (Eds)

NUMERICAL INVESTIGATION OF THE AERODYNAMIC PERFORMANCE FOR A WELLS-TYPE TURBINE IN A WAVE ENERGY CONVERTER

G. STIPCICH*, A. RAMEZANI*, V. NAVA†, I. TOUZON†, M. SANCHEZ-LARA† AND L. REMAKI*

*BCAM - Basque Center for Applied Mathematics
Mazarredo 14, E48009 Bilbao, Basque Country - Spain
e-mail: gstipcich@bcamath.org, web page: http://www.bcamath.org

†TECNALIA Research & Innovation
Parque Científico y Tecnológico de Bizkaia
C/ Geldo, Edificio 700 Derio, 20009 Spain
e-mail: vincenzo.nava@tecnalia.com, web page: http://www.tecnalia.com

Key words: Wells Turbine, Computational Fluid Dynamics, Marine Energy, Oscillating Water Column, Virtual Multiple Reference Frame

Abstract. Ocean waves constitute an extensive energy resource, whose extraction has been the subject of intense research activity in the last three decades. Among the different variants of Wave Energy Converters, the principle of the Oscillating Water Column (OWC) is one of the most promising ones. An OWC comprises two key elements: a collector chamber, which transfers the wave oscillations' energy to the air within the chamber by back and forth displacement, and a power take off system, which converts the pneumatic power into electricity or some other usable form. The Wells turbine is a self-rectifying air turbine, a suitable solution for energy extraction from reciprocating air flow in an OWC. In the present work, the steady state, inviscid flow in the Wells turbine is investigated by numerical simulations. The relatively novel Virtual Multiple Reference Frame (VMRF) technique is used to account for the rotary motion of the turbine, and the overall performance is compared with results in the literature.

1 INTRODUCTION

In the last decades, scientific and technical communities have focused their attention towards the development of novel concepts for producing electrical power from marine renewable sources. Among the various sources (stream currents, tide currents, gradient of salinity, thermal gradient, biomass, etc.), extraction of energy from waves has gained in popularity [1], and several patents for different Wave Energy Converters (WEC) have been

registered from 1980 [2]. Even though unanimous consensus on the best technology is not achieved yet, the Oscillating Water Column (OWC) is one of the most developed types of WEC, and full-size prototypes have been completed [3, 4, 5]. The OWC consists typically in a fixed-to-seabed or floating structure, which is open below the water surface, allowing water to flow in and out an internal chamber and generating oscillating compression and decompression of the air at the top of the pocket. The generated air flow passes a turbine and drives an electrical generator. Because of this bidirectional air flow, axial-flow Wells turbines [6] are used in most prototypes, having the advantage of not requiring rectifying valves.

Raghunathan [7] describes the basic principles and an interactive procedure for designing a Wells turbine for a wave energy power station. A performance analysis is provided as a function of geometric and flow parameters. Mohamed *et al.* [8] carry out an optimization process in order to increase the tangential force induced by a monoplane Wells turbine using symmetric airfoil blades. The influence of aerodynamic design on the overall plant performance (wave-to-wire model) is investigated by Brito-Melo *et al.* [9]. Modifications of the Wells turbine are proposed by Setoguchi *et al.* [10], by setting the rotor blade pitch asymmetrically at a positive pitch so as to achieve a higher mean efficiency in a wave cycle, taking into consideration that the air flow velocity is not equal in both directions. Setoguchi & Takao [11] perform a model testing and numerical simulation under irregular flow conditions of the overall performances of several kind of turbines. The authors describe the mechanism of the hysteretic behaviour in the Wells turbine. Torresi *et al.* [12] carry out extensive numerical simulations of a Wells turbine by solving the incompressible Reynolds-Averaged Navier-Stokes (RANS) equations. The authors employ three different turbulence models, and the performance results are validated with available experimental data.

In the present work, the inviscid, steady state flow in the Wells turbine is investigated by numerical simulations. The Virtual, Multiple Reference Frame technique (VMRF) [13] implemented in the Computational Fluid Dynamics (CFD) platform BBIPED [14] is used. Similarly to the Multiple Frame of Reference method (MRF) [15], different velocities can be set in different zones of the domain and the unsteady flow is approximated by a steady flow, thus saving computational cost. The main advantage of the VMRF method consists in not requiring different meshes for the different zones, making the method particularly suitable for the design optimization of the turbine in OWCs. The VMRF technique is described, and a numerical case study of a Wells turbine is carried out. The overall performance of the turbine is compared with numerical and experimental results from the literature.

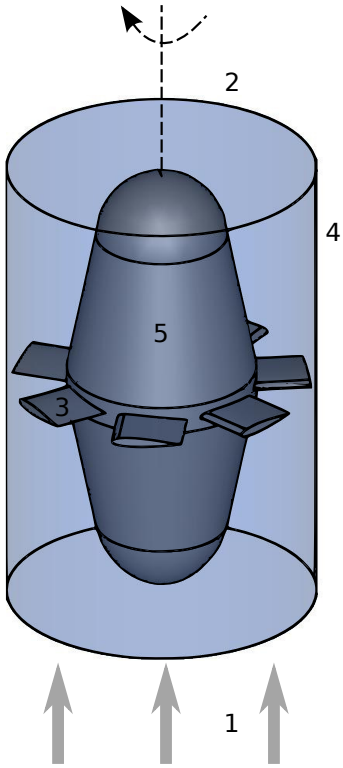

Figure 1: Sketch of the Wells turbine in the OWC. 1: inflow section; 2: outflow section; 3: seven uncambered airfoil section blades; 4: OWC cylindrical duct; 5: rotor hub.

2 NUMERICAL MODEL

2.1 The Wells turbine

Self-rectifying turbines are among the proposed solutions for an efficient and economical technique of converting the oscillating flow into an unidirectional rotary motion to drive the electric generator [16, Ch. 4.15]. The Wells turbine is the first concept of self-rectifying air turbine that have been designed [6]. The considered configuration, inspired by Torresi *et al.* [12], is sketched in Figure 1. The turbine comprises seven uncambered airfoil section blades. The blade profile is the NACA0015 with constant chord length $c = 74\,\text{mm}$, the blade chord line lies in the plane of rotation. The blade tip and rotor hub radii are, respectively, $R_{tip} = 155\,\text{mm}$ and $R_{hub} = 101\,\text{mm}$. The rotor hub length is of 240 mm on each of the two sides of the turbine, and its geometry is composed by a cone and a half sphere with radius equal to 70 mm. The OWC duct is approximated by a cylinder.

2.2 Governing equations

The compressible, three dimensional Euler equations are considered on a domain $\Omega \subset \mathbb{R}^3$ with piecewise smooth boundary $\partial\Omega$. Considering a discretization $\mathcal{T}_h$ of $\overline{\Omega}$ [17, Ch. 3.1], the integral, vector form of the governing equations with support over a control

volume $V \subset \Omega$ can be cast as [18, Ch. 2]

$$\frac{\partial}{\partial t}\int_V \mathbf{Q}\,\mathrm{d}V + \int_{\partial V} \mathbf{F}\left(\mathbf{Q}\right)\cdot\mathbf{n}\,\mathrm{d}S = \mathbf{0} \tag{1}$$

where t denotes time, and the unit vector normal to ∂V is denoted as $\mathbf{n}$. The vector of conservative variables $\mathbf{Q}$ and the non-linear mapping $\mathbf{F}\left(\mathbf{Q}\right)$ are defined, respectively, as

$$\mathbf{Q} = \begin{pmatrix} \rho \\ \rho\mathbf{u} \\ \rho E \end{pmatrix} \qquad \mathbf{F}\left(\mathbf{Q}\right) = \begin{pmatrix} \rho\mathbf{u} \\ \rho\mathbf{u}\otimes\mathbf{u} + P\mathbf{I} \\ \rho H\mathbf{u} \end{pmatrix} \tag{2}$$

where ρ and P denote, respectively, the density and static pressure, and the velocity vector is denoted by $\mathbf{u}$. The total energy and enthalpy per unit mass are denoted, respectively, by E and $H = E + P/\rho$. The symbol $\otimes$ stays for the tensor product, and $\mathbf{I}$ is the identity tensor. System (1-2) is closed by the equation of state for an ideal gas [19, Ch. 2].

2.3 Virtual multiple reference frame

In order to account for the rotary motion of the Wells turbine, the Virtual, Multiple Reference Frame technique (VMRF hereafter) is used (see Remaki *et al.* [13] for details). The VMRF method consists in an alternative algorithm of the Multiple Reference Frame model (MRF) [15]. The governing equations are transformed into a reference frame that moves with steady rotational and/or translational velocity. As a consequence, the unsteady flow in an inertial frame of reference, is approximated as a *steady* flow in the moving frame of reference. Different speeds can be assigned to different zones of the domain, and the flow in each zone is solved using the respective moving reference frame equations. The main advantage of the VMRF with respect the original MRF model is that the former does not require the creation of different meshes for the different zones.

As an example, the zone $\Omega_r \subset \Omega$ is assumed to rotate with steady angular velocity $\boldsymbol{\omega}$ and center of rotation $\mathbf{x}_0$. After a coordinate transformation into a frame of reference attached to Ω_r, system (1) results into the VMRF formulation:

$$\frac{\partial}{\partial t}\int_V \mathbf{Q}\,\mathrm{d}V + \int_{\partial V} \mathbf{F}_r\left(\mathbf{Q}\right)\cdot\mathbf{n}\,\mathrm{d}S = \int_V \mathbf{S}_r\,\mathrm{d}V \tag{3}$$

where the non-linear mapping $\mathbf{F}_r\left(\mathbf{Q}\right)$ and the source term $\mathbf{S}_r$ read as, respectively

$$\mathbf{F}_r\left(\mathbf{Q}\right) = \begin{pmatrix} \rho\left(\mathbf{u}-\mathbf{u}_r\right) \\ \rho\mathbf{u}\otimes\left(\mathbf{u}-\mathbf{u}_r\right) + P\mathbf{I} \\ \rho H\left(\mathbf{u}-\mathbf{u}_r\right) + P\mathbf{u}_r \end{pmatrix} \qquad \mathbf{S}_r = \begin{pmatrix} 0 \\ -\rho\left(\boldsymbol{\omega}\times\mathbf{u}\right) \\ 0 \end{pmatrix} \tag{4}$$

The symbol $\mathbf{u}_r$ denotes the velocity due to rotation $\mathbf{u}_r = \boldsymbol{\omega}\times\mathbf{r}$, with $\mathbf{r}$ being the position vector pointing from the center of rotation to a generic point $\mathbf{x}$ in the domain, i.e. $\mathbf{r} = \mathbf{x} - \mathbf{x}_0$.

The main advantages of the VMRF method can be summarized as follows:

- It is not required to construct different meshes for the different zones. A *single* mesh can be used for the whole computational domain Ω, as the definition of the rotating regions Ω_r takes place at solver level.

- A steady-state approximation of an unsteady problem is solved, thus saving computational cost. This approach can provide reasonable approximations of the time-averaged flow field in turbomachinery applications, where, due to the high values of the rotation velocity $\boldsymbol{\omega}$, a poor interaction between the moving and stationary zones occurs [15].

- A *single* set of equations (3-4) is used. In fact, although system (3-4) is obtained through a coordinate transformation, it provides the solution for the *absolute* values of the unknown conservative variables $\mathbf{Q}$. It can be noted that, in areas not belonging to a rotating region $V \notin \Omega_r$, the angular velocity is zero $\boldsymbol{\omega} = 0$, thus recovering the formulation (1-2) for the stationary frame of reference.

3 NUMERICAL SIMULATIONS

The BBIPED Computational Fluid Dynamics (CFD) platform [14] is used for the numerical simulation of the flow through the OWC described in Section 2.1. The platform relies on the open source packages SALOME [20], for geometry and grid generation, and on SU2 [21], for the flow solution. The BBIPED CFD platform accommodates ad-hoc implementations that are not present in the original version of the flow solver, such as the VMRF method described in Section 2.3. The aim of the present numerical experiments is to verify the applicability of BBIPED, featuring the VMRF method and a compressible solver, to be used for the solution of the relatively low speed flow in the Wells turbine (Mach number $\sim 10^{-2}$). Although the overall performance of a turbomachine may depend on phenomena associated with unsteady flow [22], this preliminary analysis accounts for the steady state only. By solving the inviscid Euler equations, the friction effects on the flow field are neglected.

3.1 Case set-up

Numerical scheme. The SU2 flow solver uses the vertex-based finite volume scheme for the space discretization [18]. The advection term is treated by a second-order accurate Roe-Turkel scheme [23], featuring a second order Venkatakrishnan limiter [24], while the source term is integrated by a first order piecewise constant method [18]. For the time marching, a second order accurate implicit Euler scheme is used. The biconjugate gradient stabilized (BCGSTAB) method [25, Ch. 9] is employed for the solution of the resulting implicit linear system of equations, and, since relatively low Mach numbers are considered, a Turkel preconditioner is employed for facilitating the convergence [26].

Computational domain. The computational domain is sketched in Figure 2. The OWC's cylindrical duct is 1400 mm long and its radius is equal to $R_{duct} = 165$ mm. The

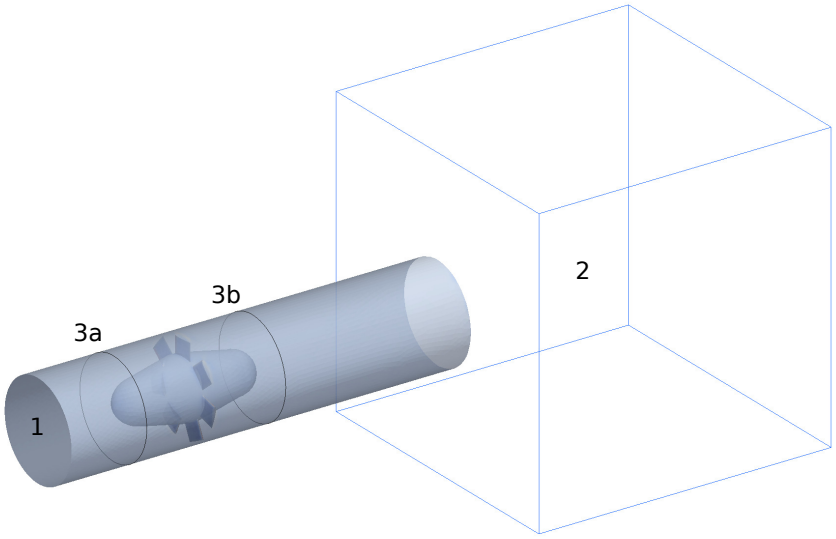

Figure 2: Sketch of the computational domain. 1: inflow section; 2: buffer region; 3a-3b: limits of the rotating region for the VMRF.

rotating region Ω_r is a cylinder whose axis coincides with the axis of rotation of the turbine, its two bases are located at a distance of 260 and 740 mm from the inflow section (labels 3a and 3b in Figure 2).

Boundary and initial conditions. At the inflow section, the imposed boundary condition is atmospheric pressure and a fixed velocity, parallel to the axis of rotation, according to the value of the considered volumetric flow rate q (see Section 3.2). In order to model a farfield boundary condition, the outflow section of the cylindrical duct opens in a wider *buffer* region, the cube E^3_{buff}, where $R_{duct} \ll E_{buff} = 1000$ mm. At the buffer faces, the imposed boundary condition is atmospheric pressure. At the duct surface and at the turbine's blades and rotor, a slip boundary condition is imposed. In the whole domain is imposed an initial condition of uniform velocity field, parallel to the axis of rotation, according the considered volumetric flow rate q (Section 3.2).

Computational meshes and convergence criteria. The whole domain is discretized by tetrahedral elements. A set of two different meshes $M1$ and $M2$ is used, with coarse and finer cell size, respectively, as specified in Table 1. In both meshes, the region included in a distance of 50 mm from the plane of rotation has an element size five times smaller than the rest of the cylindrical duct. The buffer region is discretized by using a very coarse element size, roughly fifty times larger than in the cylindrical duct. Figure 3 shows a detail of the mesh $M2$ in the vicinity of the blades.

The steady state of the flow solution is reached and the simulation is considered converged afterwards the residuals of the conserved variables $\mathbf{Q}$ have dropped of at least 3 orders of magnitude.

Table 1: Computational meshes: approximate number of elements, nodes, and size of the cells surrounding the blades with respect the airfoil chord c.

Mesh	# Tetrahedra	# Nodes	Blade cell size
$M1$	3.3×10^5	0.6×10^5	$6.8 \times 10^{-2}\, c$
$M2$	8.9×10^5	1.7×10^5	$5.4 \times 10^{-2}\, c$

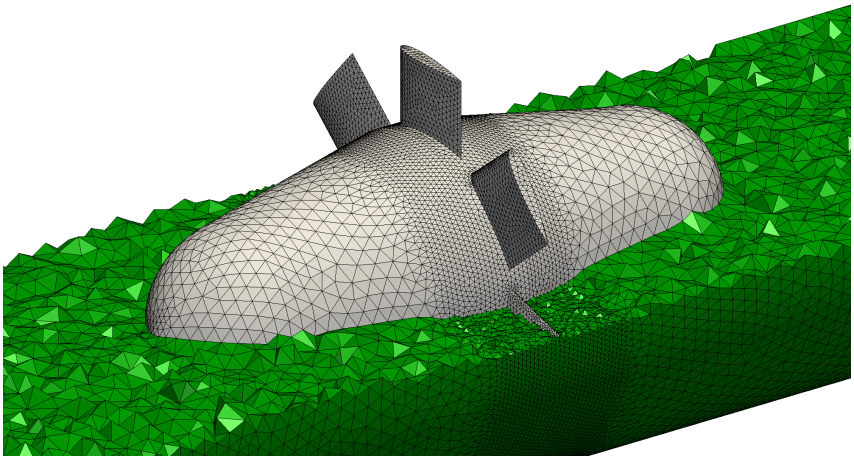

Figure 3: Detail of the tetrahedral mesh $M2$ in the vicinity of the turbine's blades.

3.2 Results

In each numerical simulation, the speed of the Wells turbine is kept constant at 2000 RPM, while a range of values for the volumetric flow rate q is considered, in order to account for different steady flow configurations [12]. The non-dimensional flow and pressure drop coefficient are defined, respectively, as

$$U^* = \frac{q}{A_{duct}\, v_{tip}} \tag{5}$$

$$\Delta P^* = \frac{\Delta P}{\rho_{ref}\, \omega_{rot}^2\, R_{tip}^2} \tag{6}$$

where A_{duct} denotes the inflow section area, the symbol v_{tip} stands for the modulus of the tangential velocity of the blade tip, the static pressure drop ΔP is evaluated at the inlet and outlet sections of the computational domain (see Figure 2), the reference density is assumed equal to $\rho_{ref} = 1.225\,\mathrm{kg/m^3}$, and the symbol ω_{rot} denotes the speed of the Wells turbine, expressed in rad/s.

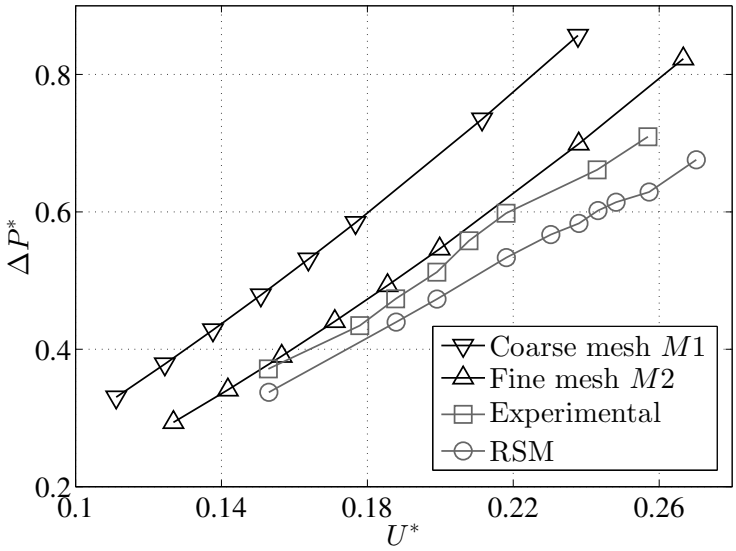

Figure 4: Non-dimensional pressure drop coefficient for different values of the flow coefficient, obtained by the BBIPED platform on two different meshes $M1$ and $M2$ (Table 1). Both experimental and RSM results by Torresi *et al.* [12] are shown for reference.

Figure 4 shows the plot of the non-dimensional pressure drop coefficient for different values of the flow coefficient. For comparison, both experimental and numerical results by Torresi *et al.* [12] are included. In the investigation of Torresi *et al.* [12], the Reynolds-Averaged Navier-Stokes (RANS) are solved, using a Launder Reynolds-stress turbulence model (RSM) [27]. The following conclusions can be drawn:

- By the use of the finer mesh $M2$, the accuracy of the calculated pressure drop coefficient is significantly increased. A good matching of the calculated pressure drop with the experimental results is observed especially for lower values of the inlet flow $U^* < 0.22$. Thus the overestimation of the pressure drop obtained by BBIPED is to be addressed principally to the use of coarse meshes in this preliminary study. As a matter of fact, in the numerical simulations of Torresi *et al.* [12], computational meshes of about 2×10^6 cells are considered, and only one seventh of the domain (one blade) is computed, taking advantage of the tangential symmetry. Considering the number of degrees of freedom used, it can be determined that Torresi *et al.* [12] employ roughly $(2 \times 10^6 \times 7) \,/\, (1.7 \times 10^5) \simeq 80$ times more degrees of freedom than the fine mesh $M2$ (see Table 1).

- A linear trend of the pressure drop coefficient is coherently observed. The Wells turbine is known to exhibit a roughly linear relationship between the turbine pressure drop and the volumetric flow rate [9, 16].

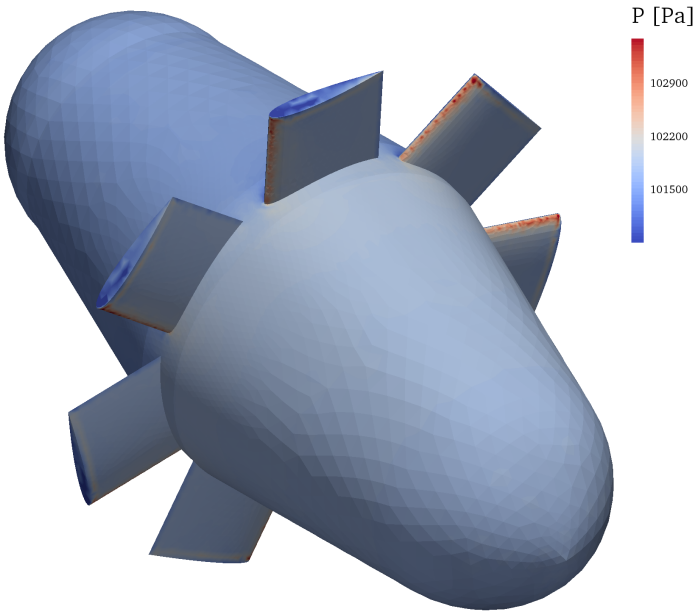

Figure 5: Distribution of the static pressure P over the surface of the Wells turbine.

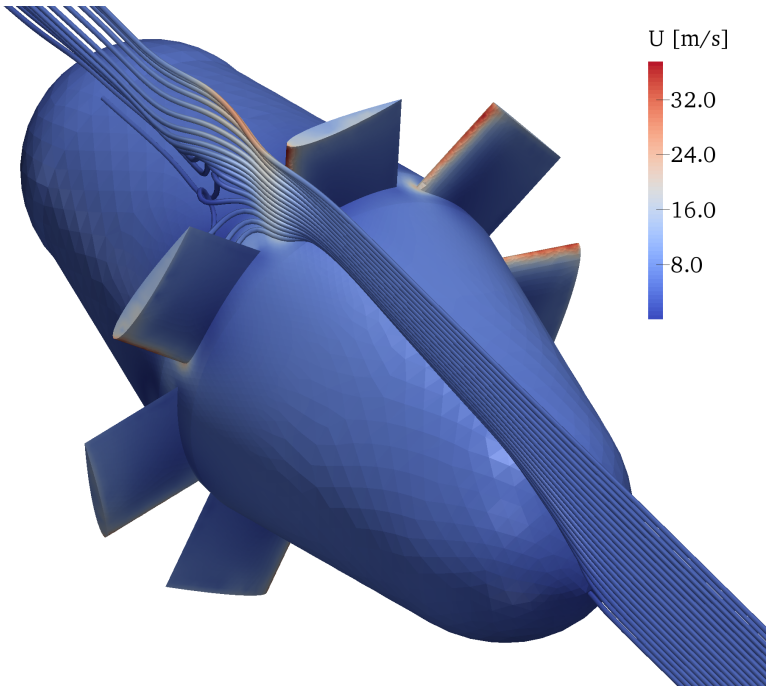

Figure 6: Distribution of the velocity magnitude over the surface of the Wells turbine. Velocity streamlines are plotted, radially distributed with respect the rotation axis.

Figure 5 shows the distribution of the static pressure P over the surface of the Wells turbine, for $U^* \approx 0.13$ and using mesh $M2$. The pressure distribution is higher on the leading edge and lower on the trailing edge, coherently with the sense of rotation of the turbine.

Figure 6 shows the distribution of the velocity magnitude over the surface of the Wells turbine, along with a number of velocity streamlines, radially distributed with respect the rotation axis, for $U^* \approx 0.13$ and using mesh $M2$. The flow is coherently deviated towards the direction of the rotary motion of the turbine, accelerating past the blades.

4 CONCLUSIONS

The aerodynamic performance of a Wells-type turbine is investigated by numerical simulations of the steady flow inside an OWC. The three-dimensional, compressible Euler equations are solved by using the CFD platform BBIPED. The novel technique of the Virtual Multiple Reference Frame (VMRF) is used to account for the rotary motion of the turbine. By setting different velocities in different zones of the domain, the VMRF method allows for approximating the unsteady flow with a steady solution, thus saving computational cost. Moreover, since no different meshes are required for the different zones, the meshing operation is considerably facilitated. In all the performed numerical tests, a relatively low Mach number $\sim 10^{-2}$ is considered, and a compressible flow solver with preconditioning is successfully employed. The performance of the Wells turbine, evaluated by means of the pressure drop between inlet and outlet sections, are in satisfactory agreement with both experimental and numerical tests in the literature.

Acknowledgment

This research is partially supported by Diputación Foral de Bizkaia under Grant BFA/DFB-6/12/TK/2012/00020, by the Basque Government through the BERC 2014-2017 program and by the Spanish Ministry of Economy and Competitiveness MINECO: BCAM Severo Ochoa accreditation SEV-2013-0323.

Goran Stipcich was partially funded by the Project of the Spanish Ministry of Economy and Competitiveness with reference MTM2013-40824-P.

Vincenzo Nava's work has been funded by the European Commission through the project TIFER (PEOPLE-2010-COFUND; grant n° 267200) and co-funded by the Spanish Ministry of Economics and Competitiveness through the measure MINECO (COFUND-2013-40277).

References

[1] Falcão, A. F. de O. Wave Energy Utilization: A Review of the Technologies. *Renewable and Sustainable Energy Reviews* **14**, 899–918 (2010).

[2] McCormick, M. E. *Ocean Wave Energy Conversion* (Wiley & Sons, New York, 2007).

[3] Heath, T., Whittaker, T. J. T. & Boake, C. B. The Design, Construction and Operation of the LIMPET Wave Energy Converter (Islay, Scotland). In *Proceedings of 4th European Wave Energy Conference*, 49–55 (2001).

[4] Falcão, A. F. de O. The Shoreline OWC Wave Power Plant at the Azores. In *Proceedings of 4th European Wave Energy Conference*, 42–48 (2001).

[5] Torre-Enciso, Y., Ortubia, I., López de Aguileta, L. I. & Marqué, J. Mutriku Wave Power Plant: from the thinking out to the reality. In *Proceedings of 8th European Wave and Tidal Energy Conference*, 319–329 (2009).

[6] Wells, A. A. *Fluid Driven Rotary Transducer. British Patent 1595700* (1976).

[7] Raghunathan, S. A Methodology for Wells Turbine Design for Wave Energy Conversion. *Proceedings of the Institution of Mechanical Engineers, Part A: Journal of Power and Energy* **31**, 221–232 (1995).

[8] Mohamed, M. H., Janiga, G., Pap, E. & Thévenin, D. Multi-Objective Optimization of the Airfoil Shape of Wells Turbine Used for Wave Energy Conversion. *Energy* **36**, 438–446 (2011).

[9] Brito-Melo, A., Gato, L. M. C. & Sarmento, A. J. N. A. Analysis of Wells Turbine Design Parameters by Numerical Simulation of the OWC Performance. *Ocean Engineering* **29**, 1463–1477 (2002).

[10] Setoguchi, T., Santhakumar, S., Takao, M., Kim, T. H. & Kaneko, K. A Modified Wells Turbine for Wave Energy Conversion. *Renewable Energy* **28**, 79–91 (2003).

[11] Setoguchi, T. & Takao, M. Current Status of Self Rectifying Air Turbines for Wave Energy Conversion. *Energy Conversion and Management* **47**, 2382–2396 (2006).

[12] Torresi, M., Camporeale, S. M. & Pascazio, G. Detailed CFD Analysis of the Steady Flow in a Wells Turbine Under Incipient and Deep Stall Conditions. *Journal of Fluids Engineering* **131** (2009).

[13] Remaki, L., Ramezani, A., Blanco, J. M. & Antolin, J. I. Efficient Rotating Frame Simulation in Turbomachinery. In *Proceedings of ASME Turbo Expo 2014: Turbine Technical Conference and Exposition*, vol. 2B (2014).

[14] BCAM - Basque Center for Applied Mathemathics. BBIPED, CFD Industrial Platform for Engineering Design (2015). URL `http://www.bcamath.org/es/research/lines/CFDMS/software`.

[15] Luo, J. Y., Issa, R. I. & Gosman, A. D. Prediction of Impeller-Induced Flows in Mixing Vessels Using Multiple Frames of Reference. In *I ChemE Symposium Series*, vol. 136, 549–556 (1994).

[16] Dixon, S. L. *Fluid Mechanics and Thermodynamics of Turbomachinery* (Elsevier Butterworth-Heinemann, Boston, 2013), 5th edn.

[17] Quarteroni, A. & Valli, A. *Numerical Approximation of Partial Differential Equations* (Springer-Verlag Italia, Milano, 1994).

[18] Blazek, J. *Computational Fluid Dynamics: Principles and Applications* (Elsevier, Amsterdam, 2001), 2nd edn.

[19] Anderson, J. D. *Computational Fluid Dynamics* (Mc Graw Hill, New York, 1995), 3rd edn.

[20] OPEN CASCADE. SALOME, The Open Source Integration Platform for Numerical Simulation (2015). URL `http://www.salome-platform.org/`.

[21] Stanford University Aerospace Lab. SU2, The Open-Source CFD Code (2015). URL `http://su2.stanford.edu/index.html`.

[22] Greitzer, E. M. Introduction to Unsteady Flow in Turbomachines. In *Von Karman Inst. for Fluid Dynamics Unsteady Flow in Turbomachines*, vol. 1 (1984).

[23] Viozat, C. Implicit Upwind Schemes for Low Mach Number Compressible Flows. Tech. rep., Institut National de Recherche en Informatique et en Automatique (1997).

[24] Venkatakrishnan, V. On The Accuracy of Limiters and Convergence to Steady State Solutions. Tech. Rep. AIAA-93-088, American Institute of Aeronautics and Astronautics (1993).

[25] van der Vorst, H. A. *Iterative Krylov Methods for Large Linear Systems* (Elsevier Butterworth-Heinemann, New York, 2003).

[26] Turkel, E. Preconditioning Techniques in Computational Fluid Dynamics. In *Annual Review of Fluid Mechanics*, vol. 31, 385–416 (1999).

[27] Launder, B. E. Second-Moment Closure and its Use in Modelling Turbulent Industrial Flows. *International Journal for Numerical Methods in Fluids* **9**, 963–985 (1989).